PMSM Design for Achieving a Target Torque-Speed-Efficiency Map

Carlos Candelo-Zuluaga, Antonio Garcia Espinosa, Jordi-Roger Riba, Pere Tubert Blanch

***Abstract*— During the last years, the requirements for a fast and reliable design of electrical machines by applying optimization methods using finite element analysis (FEA), has become a subject of study. Due to their capabilities, permanent magnet synchronous machines (PMSMs) have become the preference choice for many applications, including electric vehicles (EVs) propulsion, water-pumping, robotics, or renewable power generation among others. This paper presents a novel methodology for designing and optimizing PMSMs using the torque-speed-efficiency map. The design-optimization algorithm requires as input, the torque-speed-efficiency map of the target motor, to define the required performance for the given application. The objective is to find the motor geometry which better approximates the target torque-speed-efficiency map. The PMSM is evaluated by using magneto-static FEA combined with direct-quadrature *(d-q)* electrical modeling, thus greatly reducing the computational burden when compared to conventional time-dependent FEA methods. The magneto-static FEA method calculates iron losses taking into account the magnetic flux density harmonic content by applying a time-space conversion approach. The design-optimization process takes into account the control strategy as well as losses separation, which is validated by using the public experimental data of the Toyota Prius and Camry PMSMs.**

***Index Terms*—Permanent magnet machines, Design optimization, Design tools, Magnetic losses, Finite element analysis**

NOMENCLATURE

B_{xy}	Magnetic flux density in a defined region [T]
d_{wire}	Wire diameter [m]
D_{ir}	Inner rotor diameter [m]
D_{is}	Inner stator diameter [m]
D_{or}	Outer rotor diameter [m]
D_{os}	Outer stator diameter [m]
f_{obj}	Objective function [-]
g	Air gap length [m]
h_{brg}	Rotor bridge height [m]
h_{PM}	Permanent magnet height [m]
h_{rib}	Rotor rib height [m]
h_{so}	Slot opening height [m]
h_{sy}	Stator yoke height [m]
h_t	Tooth height [m]
I_{max}	Maximum current [A_{RMS}]
L	Stack lamination length [m]
L_d	Direct axis inductance [H]
L_q	Quadrature axis inductance [H]
m	Number of stator phases [-]
n	Mechanical angular velocity [rpm]
N_{ph}	Number of phase turns [-]
P_U	Output power [W]
P_{Fe}	Iron losses [W]
P_{ML}	Mechanical Losses [W]
P_{Cu}	Copper Losses [W]
p	Pole pairs [-]
q	Number of slots per pole and phase [-]
R_{Fe}	Iron resistance [Ω]
R_s	Phase winding resistance [Ω]
T	Output torque [N·m]
U_{dc}	DC bus voltage [V]
w_{brg}	Rotor bridge width [m]
w_{PM}	Permanent magnet width [m]
w_{so}	Slot opening width [m]
w_t	Tooth width [m]
w_{web}	Rotor web width [m]
α_{PM}	V-shape permanent magnet angle [rad]
η	Efficiency [p.u.]
θ_e	Electrical angle [rad]
θ_m	Mechanical angle [rad]
ω_e	Electrical angular velocity [rad/s]
Ψ_{abc}	Phase flux linkage [V·s]
Ψ_{PM}	Permanent magnet flux linkage [V·s]
Ψ_{sd}	Direct axis flux linkage [V·s]
Ψ_{sq}	Quadrature axis flux linkage [V·s]

C. Candelo, A. Garcia and J. Riba are with the Electrical Engineering Department, Universitat Politècnica de Catalunya, Barcelona 08034, Spain (e-mail: carlos.andres.candelo@upc.edu; antoni.garcia@upc.edu; jordi.riba-ruiz@upc.edu). P. Tubert is with the mechanical engineering department, Midtal Talentos S.L, Banyoles 17820, Spain (e-mail: pere.tubert@midtal.net).

I. INTRODUCTION

ELECTRICAL machines design and optimization areas are demanding faster and more reliable algorithms. Considering electric vehicle (EV) applications, PMSMs require special attention due to their superior capabilities compared to other machines [1]. Focusing on the electrical machines design and optimization area, some earlier studies tried to couple design approaches with FEA, in order to maximize the efficiency of the machine within the frequent operating points of the electric vehicle according to a given driving cycle [2]. However, due to the high FEA computational burden, the optimization in [2] was focused on a reduced number of geometric parameters. Some improvements were done in posterior studies [3], by coupling magneto-static FEA analysis with lumped circuit modelling. In the same way [4], [5] applied a magneto-static analysis approach combined with the application of reluctance networks. Nevertheless, [3]–[5] do not consider the harmonic content of iron losses, thus attaining limited precision at high frequencies. However, the studies based on magneto-static FEA, instead of considering the whole torque-speed area, only analyze a reduced number of operating points and do not take into account different control strategies.

The first studies proposing fast FEA methods using magneto-static analysis were based on the so called space-time transformation [6]. Posterior studies in this area, applied this method to analyze the drive cycle performance of a traction PMSM [7]. Other studies model and optimize brushless doubly-fed induction machines [8]. In [9], a computationally-efficient FEA (CE-FEA) approach based on the pseudo rotating position (PRS) is presented, which allows comparing the performance of different optimization techniques based on the resulting PMSM design. Some other research works were based on designing and optimizing motor performances by only considering the rated conditions [10]. For example, [11] presents a methodology to improve the rated output power without increasing the material cost. Some other studies analyze a reduced number of points of a known driving cycle [12].

There are studies related to design and optimization techniques focused on optimizing the efficiency distribution within a certain operating area. For example, [13] proposes an optimal design combining FEA and mesh adaptive direct search (MADS) algorithm to attain maximum efficiency distribution in the maximum consumption areas of a heavy duty electric vehicle (HD-EV). In [14], a multi-criteria design and optimization methodology is proposed for being applied to a PMSM, while considering the full drive cycle using some efficiency points.

The methodology proposed in this study provides a new design and optimization approach for PMSMs using the torque-speed-efficiency map. To this end, the efficiency distribution within the torque-speed domain is defined before starting the design-optimization process, allowing to customize the motor performance for the required application. The reference torque-speed-efficiency map can be defined within the whole or a selected region of the torque-speed map. The design-optimization process adjusts the values of the geometrical variables to achieve the required efficiency distribution within the considered torque-speed area. This method uses a novel ultra-fast magneto-static FEA model combined with *d-q* electrical modelling, thus greatly reducing the computational burden when compared to conventional methods based on time-dependent FEA. The proposed FEA electromagnetic analysis method allows computing power losses, specifically the iron losses, taking into account the contribution of the spatial harmonics of the magnetic flux density. Another important feature of the proposed algorithm, is the possibility to obtain different performance characteristics of the PMSM during the design process, while considering different control strategies.

This paper is organized as follows. Section II presents the proposed PMSM design and optimization methodology, explaining in detail the process and the required inputs and outputs. Section III develops the procedure to determine the iron losses from the magneto-static FEA. Section IV details the process to compute the efficiency map by using a *d-q* electrical model. Section V validates the magneto-static FEA model by comparing the obtained efficiency map with the one found in the public experimental data of Toyota Prius 2004 PMSM. Section VI validates the design-optimization process based on the same Toyota Prius 2004 [15] and Camry 2007 [16] PMSMs, by determining the motor geometry that better matches with the experimental torque-speed-efficiency map, i.e., the closest geometry to the original one. Finally, Section VII develops the conclusions.

II. PMSM Design and Optimization Methodology

This section develops the methodology to compute from a given efficiency map and some constraints, the geometry of the PMSM.

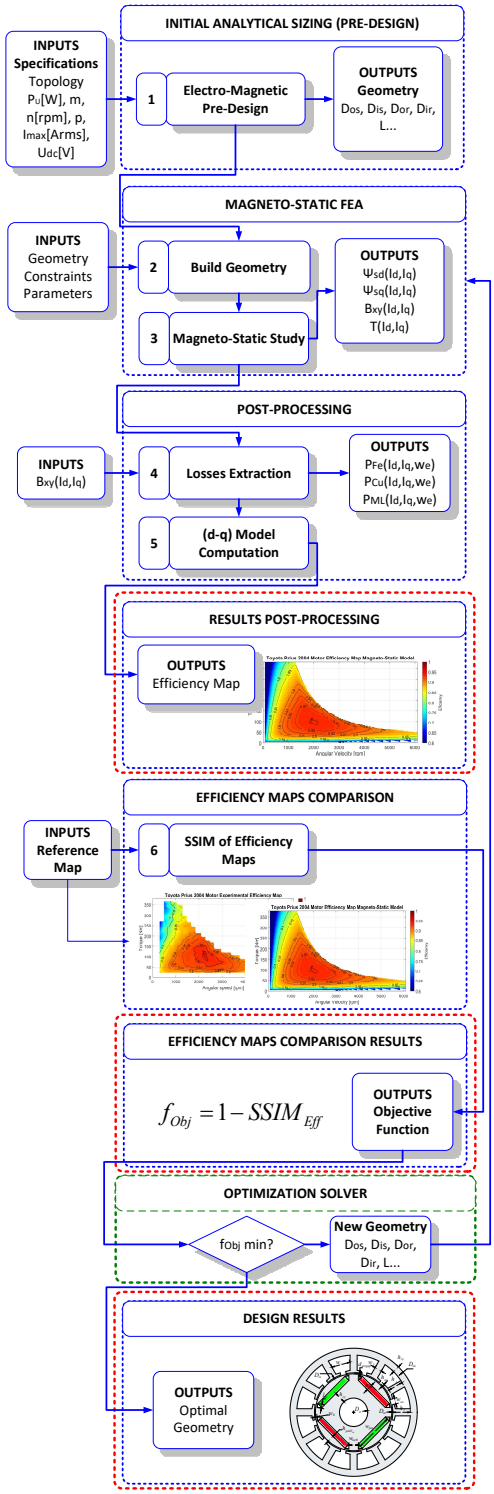

Fig. 1. Permanent magnet synchronous motor design and optimization algorithm.

This methodology is divided in six steps. The first step performs an initial sizing of the motor geometry (pre-design) by applying analytical equations and some general rules. Next, this initial geometry is introduced into the FEA interface. Taking this first input and the physical constraints, the geometry is analyzed by means of a magneto-static FEA study. From this study the flux linkage, stator magnetic flux density distribution and electromagnetic torque can be extracted. From all this information, the losses (mechanical, magnetic and Joule losses) can be computed as a function of the frequency and the angle and amplitude of the current. To obtain the efficiency map covering all torque-speed region, the *d-q* electric model is used. Finally, the structural similarity index SSIM, which is an image comparison technique [17], is applied to compare the obtained torque-speed-efficiency map with the target one. This process is detailed in Fig. 1.

A. Electromagnetic Pre-Design and Geometry Computation

The first step consists in calculating an initial geometry by using analytical equations and some general rules [18]. The aim of this step is to obtain a seed geometry as close as possible to the optimal one. Therefore, the constraints set and parameters obtained at this point are important.

The second step consist in evaluating the geometry, its correctness and feasibility, which is built in the FEA environment.

B. Magneto-Static Study

The third step consist in performing the magneto-static FEA study of the given geometry. First, the positive direct axis of the rotor, where the PM flux is pointing outwards radially, is aligned with the reference phase, i.e., phase *a*. Once the rotor is aligned, the current space vector is injected towards the negative direct axis and the magneto-static FEA simulation is performed. Next, the rotor and its corresponding current space vector are shifted by half of a slot, and another magneto-static FEA simulation is carried out with the same current space vector. This same process is repeated for different amplitudes and angles of the current space vector within the motoring quadrant.

Fig. 2 details the algorithm applied to determine the amplitudes and angles of the current space vector in the magneto-static FEA simulations to determine the torque, stator magnetic flux density and flux linkage required to build the efficiency-torque-speed map for steady-state conditions using the *d-q* model.

1: Set the Current magnitude and angle steps:
$i_s = 0 : \Delta i_s : i_{s\max}$, $\theta_e = \pi : \Delta\theta_e : \pi/2$
2: Set the mechanical angle steps: $\theta_m = 0 : \Delta\theta_m : \tau_s / 2$
3: **for** $\theta_e = \pi$ to $\theta_e = \pi/2$ **do**
4: **for** $i_s = 0$ to $i_s = i_{s\max}$ **do**
5: **for** $\theta_m = 0$ to $\theta_m = \tau_s / 2$ **do**
6: Magneto-Static Analysis
7: **end**
8: **end**
9: **end**

Fig. 2. Magneto-static study algorithm.

C. Copper, Iron and Mechanical Losses Extraction

When applying the magneto-static analysis to determine the PMSM performance (voltages, currents, power factor, efficiency, etc.), calculation of power losses becomes a challenging point. The three main losses to consider are the copper resistance, magnetic lamination and mechanical losses due to friction and vibration. They are calculated in the post-processing stage (see Fig. 1) from the data provided by the magneto-static analysis.

The phase resistance is needed to compute copper losses. The FEA software provides a fast calculation of this parameter for ambient conditions. As the process is meant to be a fast design and optimization tool, the effect of temperature is initially neglected, although, the designer can specify the expected winding temperature, which depends on the final application.

The Bertotti model is used to compute the iron losses,

$$P_{Fe-Eddy} = \frac{\sigma \cdot h^2}{12 \cdot T} \cdot \int_0^T \int_{d\forall} \left(\frac{dB}{dt} \right)^2 \cdot d\forall \cdot dt \tag{1}$$

$$P_{Fe-Hyst} = \frac{K_h \cdot \rho}{T} \cdot \int_{d\forall} B_m{}^{\alpha} \cdot \left(1 + \sum_{i=1}^{n} \frac{\beta}{B_m} \cdot (\Delta B_i) \right) \cdot d\forall \tag{2}$$

$$P_{Fe-Excess} = \frac{K_{exc} \cdot \rho}{T} \cdot \int_0^T \int_{d\forall} \left(\left| \frac{dB}{dt} \right| \right)^{1.5} \cdot d\forall \cdot dt \tag{3}$$

σ being the electrical conductivity of the iron laminations, h the thickness of the iron laminations, $d\forall$ the differential volume of analysis, T the time period of the wave formed in one volume, K_h the hysteresis constant, dt the differential time, ρ the mass per unit volume of the iron laminations, α and β the hysteresis exponent and minor loop constant, respectively, and K_{exc} the excess constant. This step is further detailed in Section III.

Mechanical losses mainly depend on bearings friction and rotor size. The effect of vibration on such losses can be calculated by using an external model [1], [19].

D. d-q Model Computation and Efficiency-Torque-Speed Maps Comparison

The *d-q* electrical model under the quasi-static approximation is used to calculate the operating characteristics of the PMSM under steady state conditions. One of the strongest points of using *d-q* modeling is the possibility to compute the operating characteristics by imposing the control strategy. The *d-q* model is explained in detail in Section IV.

Once the efficiency-torque-speed map of the current geometry has been obtained from the *d-q* electrical model, it is necessary to compare how close it is with respect to the target or reference map. To this end, the structural similarity index SSIM is applied [17], [20]. This index returns a normalized value between 0 and 1 to indicate the degree of similarity between two images. SSIM considers three main aspects, i.e., the point-to-point difference, the standard deviation and the structural similarity between all points in both maps.

E. Optimization Solver

After calculating the SSIM index, the objective function of the optimization process is calculated as 1-SSIM. This value is the input of the solver used during the optimization stage, which calculates the different geometric dimensions of the machine. The *pattern search* solver from Matlab® is used in

this study, which combined with a multiple start algorithm, pursues finding the global minimum of the objective function according to the specified constraints. This algorithm is suitable for non-continuous and non-differentiable objective functions, as the one applied in this work, since some solutions are not physically feasible and thus, it is not possible to evaluate the SSIM index. Fig. 3 shows the *pattern search* optimization solver algorithm.

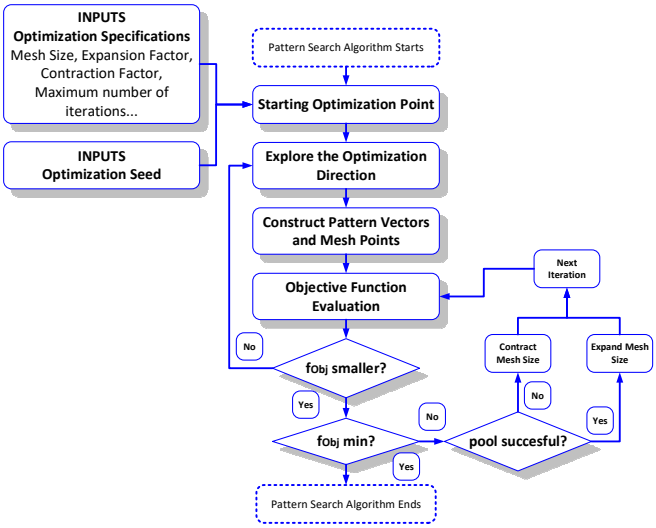

Fig. 3. Pattern Search optimization solver algorithm.

Table I shows the PMSM optimization geometric parameters.

TABLE I
OPTIMIZATION GEOMETRIC PARAMETERS

Geometric Parameter	Description
d_{wire}	Wire diameter [m]
D_{ir}	Inner rotor diameter [m]
D_{is}	Inner stator diameter [m]
D_{or}	Outer rotor diameter [m]
D_{os}	Outer stator diameter [m]
g	Air gap length [m]
h_{brg}	Rotor bridge height [m]
h_{PM}	Permanent magnet height [m]
h_{rib}	Rotor rib height [m]
h_{so}	Slot opening height [m]
h_{sy}	Stator yoke height [m]
h_t	Tooth height [m]
L	Stack lamination length [m]
N_{ph}	Number of phase turns [-]
w_{brg}	Rotor bridge width [m]
w_{PM}	Permanent magnet width [m]
w_{so}	Slot opening width [m]
w_t	Tooth width [m]
w_{web}	Rotor web width [m]
α_{PM}	V-shape permanent magnet angle [rad]

III. IRON LOSSES CALCULATION FROM THE MAGNETO-STATIC ANALYSIS

Iron losses calculation using magneto-static FEA simulations becomes a great challenge. The problem arises when using time-dependent Bertotti equations, since they assume the time dependence of the magnetic flux density for every finite element within the analyzed domain. As the aim is using magneto-static FEA due to computational constraints, which does not provide such time dependence, this study proposes a new method for computing the iron losses. The proposed method takes into account the spatial distribution of the magnetic flux density to predict the time evolution. This method avoids to apply loss function modeling to compute the efficiency maps [21], which for some cases would be useful, but when searching high accuracy to compute the operational characteristics, it is not the most suitable choice. The *B-H* curve of the magnetic iron laminations is included in the magneto-static FEA study, so saturation effects are considered.

A. Magnetic Flux Density Distribution

To evaluate the magnetic flux density distribution, two main regions are analyzed, i.e., the stator tooth and the yoke. Each region is defined as a repeatable part along the stator periodicity. They are studied to monitor the evolution of the magnetic flux density along the stator. The magnetic flux density of every finite element is integrated within the stator tooth and yoke domains to determine the magnetic flux spatial distribution as,

$$\int_{s} \frac{B_{\Delta}}{s_{\Delta}} \cdot ds \tag{4}$$

ds being the differential surface, s_{Δ} the finite surface composed by the finite elements of the mesh and B_{Δ} the mean magnetic flux density within each finite surface s_{Δ}. Fig. 4 (a) shows the discrete spatial magnetic flux density distribution over the analyzed stator teeth and yoke regions. Fig. 4 (b) displays the spatial distribution of the magnetic flux density by integrating the analyzed regions. This example uses the PMSM Toyota Prius 2004 when i_d = -270 A and i_q = 270 A.

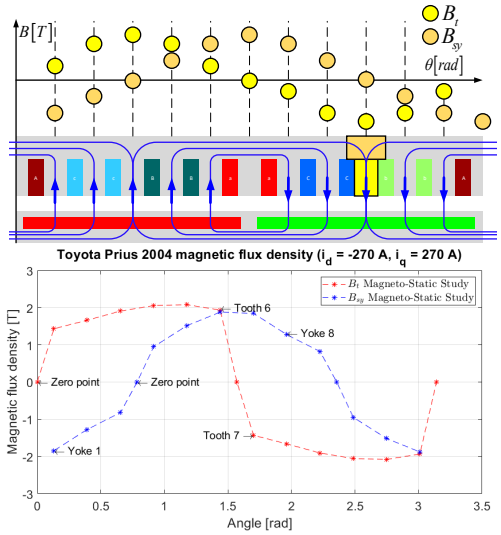

Fig. 4. (a) Discrete spatial magnetic flux density distribution over the stator teeth and yoke regions. (b) Toyota Prius 2004 magnetic flux density distribution at id = -270 A and iq = 270 A.

The main hypothesis under this assumption is that the time variation of the magnetic vector potential is almost negligible due to the reduced value of the electrical frequency range of the motor, and so, the values of the magnetic vector potential in the time domain are equivalent to that of the static domain.

$$\frac{1}{\mu}\cdot\left(\frac{\partial^2 A}{\partial x^2}+\frac{\partial^2 A}{\partial y^2}\right)=-J+\frac{\partial A}{\partial t}\cdot\sigma \tag{5}$$

Therefore, the term $(\partial A/\partial t)\cdot\sigma$ is neglected within the frequencies of study. It is noted that when modeling ferromagnetic materials using standard two dimensional FEA, eddy currents are also neglected.

B. Harmonic Wave Decomposition

Once the space distribution of the magnetic flux density is obtained, the equivalent wave is decomposed in harmonic components.

The time-space conversion is applied to transform time domain Bertotti's equations into space distribution equivalent equations as follows,

$$\left(\frac{dB}{d\theta_e}\right)=\left(\frac{dB}{dt}\right)\cdot\left(\frac{dt}{d\theta_e}\right)\rightarrow\left(\frac{dB}{dt}\right)=\left(\frac{dB}{d\theta_e}\right)\cdot\omega_e \tag{6}$$

The magnetic flux density integration in (4) can be incorporated in the Bertotti equations together with the time-space conversion. The modified Bertotti equations to calculate iron losses using magneto-static FEA result in,

$$P_{Fe-Eddy}=\frac{\sigma\cdot h^2}{12\cdot T}\cdot\omega_e^{\,2}\cdot\int_0^T\int_{d\forall}\left(\frac{d\int_s\frac{B_\triangle}{s_\triangle}\cdot ds}{d\theta_e}\right)^2\cdot d\forall\cdot d\theta_e \tag{7}$$

$$P_{Fe-Hyst}=\frac{K_h\cdot\rho}{T}\cdot\int_{d\forall}\left(\int_s\frac{B_\triangle}{s_\triangle}\cdot ds\right)_m^{\alpha}\cdot\left(1+\sum_{i=1}^{n}\frac{\beta}{\left(\int_s\frac{B_\triangle}{s_\triangle}\cdot ds\right)_m}\cdot\left(\Delta\left(\int_s\frac{B_\triangle}{s_\triangle}\cdot ds\right)_i\right)\right)\cdot d\forall \tag{8}$$

$$P_{Fe-Excess}=\frac{K_{exc}\cdot\rho}{T}\cdot\omega_e^{1.5}\cdot\int_0^T\int_{d\forall}\left|\frac{d\left(\int_s\frac{B_\triangle}{s_\triangle}\cdot ds\right)}{d\theta_e}\right|^{1.5}\cdot d\forall\cdot d\theta_e \tag{9}$$

The frequency domain expression of the hysteresis term is,

$$P_{Fe-Hyst}=K_h\cdot\rho\cdot f\cdot\hat{B}^{\alpha}\cdot\forall \tag{10}$$

IV. *d-q* Model Computation

The *d-q* (direct-quadrature) electrical model is selected to compute the whole operational regime of the PMSM within the torque-speed plane, which is shown in Fig. 5.

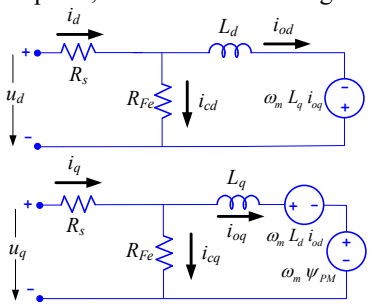

Fig. 5. (*d-q*) electrical model.

For this purpose, the quasi-static equations are used [22]. This electrical model allows selecting the control strategy, thus allowing to evaluate different control strategies, presenting a huge advantage over other available models [23].

The *d-q* flux linkages are obtained from the magneto-static analysis,

$$\begin{cases}\psi_d=\psi_{PM}+L_d\cdot i_{od}\\ \psi_q=L_q\cdot i_{oq}\end{cases} \tag{11}$$

The back electromotive force (BEMF) can be obtained from the flux linkage as a function of the angular velocity as,

$$\begin{cases}u_{od}=-\omega_e\cdot L_q\cdot i_{oq}=-\psi_q\cdot\omega_e\\ u_{oq}=\omega_e\cdot\left(L_d\cdot i_{od}+\psi_{PM}\right)=\psi_d\cdot\omega_e\end{cases} \tag{12}$$

Currents i_{od} and i_{oq} are selected taking into account the control strategy.

As the magnetic losses have been previously evaluated, they can be modelled by means of a parallel resistance.

$$R_{Fe}=m\cdot\left(u_{od}^{\,2}+u_{oq}^{\,2}\right)/\left(2\cdot P_{Fe}\right) \tag{13}$$

Currents i_{cd} and i_{cq} are calculated from the iron resistance,

$$\begin{cases}i_{cd}=u_{od}/R_{Fe}\\ i_{cq}=u_{oq}/R_{Fe}\end{cases} \tag{14}$$

Total current i_d and i_q are calculated from currents i_{cd}, i_{cq}, i_{od} and i_{oq}. The voltage equations are as follows,

$$\begin{cases}u_d=R_s\cdot i_d+L_d\cdot\frac{d}{dt}\cdot i_{od}-\omega_e\cdot L_q\cdot i_{oq}\\ u_q=R_s\cdot i_q+L_q\cdot\frac{d}{dt}\cdot i_{oq}+\omega_e\cdot L_d\cdot i_{od}+\omega_e\cdot\Psi_{PM}\end{cases} \tag{15}$$

Fig. 6 details the applied procedure to compute the efficiency-torque-speed maps from the magneto-static FEA data combined with the *d-q* electrical model.

1: Extract magneto-static FEA data:
$\psi_a\left(i_d,i_q\right),\psi_b\left(i_d,i_q\right),\psi_c\left(i_d,i_q\right),B_{xy}\left(i_d,i_q\right),T\left(i_d,i_q\right),R_s$
2: Extract losses from magneto-static FEA data:
$P_{Fe}\left(i_d,i_q,f\right),P_{ML}\left(f\right),P_{Cu}\left(i_d,i_q\right)$
3: Torque-speed domain discretization: $T=0:\Delta T:T_{\max}$, $\omega_e=0:\Delta\omega_e:\omega_{e\max}$
4: Control strategy selection (MTPA, ME or MTPV)
5: Compute BEMF for all ω_e: $u_{oq}=\psi_d\cdot\omega_e$, $u_{od}=\psi_q\cdot\omega_e$
6: Compute iron resistance R_{Fe} for all ω_e: $R_{Fe}=m\cdot\left(u_{od}^{\,2}+u_{oq}^{\,2}\right)/\left(2\cdot P_{Fe}\right)$
7: Compute *d-q* iron currents i_{cd}, i_{cq} for all ω_e: $i_{cd}=u_{od}/R_{Fe}$, $i_{cq}=u_{oq}/R_{Fe}$
8: Compute *d-q* currents i_d, i_q for all ω_e: $i_d=i_{od}+i_{cd}$, $i_q=i_{oq}+i_{cq}$
9: Compute copper losses for all ω_e: $P_{Cu}=\left(m/2\right)\cdot R_s\cdot\left(i_d^{\,2}+i_q^{\,2}\right)$
10: Selection of the magnitudes from control strategy

Fig. 6. (*d-q*) model computation to obtain operational characteristics taking into account the control strategy.

V. Magneto-Static FEA Model Validation

The experimental data of the PMSM of the Toyota Prius 2004 [15] is used to validate the proposed magneto-static FEA combined with the *d-q* electrical model. To this end, the public data of the Toyota Prius (geometric dimensions, voltages and currents in the torque-speed map, materials, power losses, temperature, etc.) are used as the input of the proposed model. Next, through the model proposed here, a discrete efficiency-torque-speed map is obtained, which is compared with the experimental one. Fig. 7 (a) shows the experimental efficiency map, whereas Fig. 7 (b) shows the efficiency map obtained through the approach proposed in this paper.

Ten randomly chosen points are considered to compare both maps. Table I shows the angular velocity, torque and

efficiency corresponding to each point. Thus, the relative error between the model and the experimental data is provided.

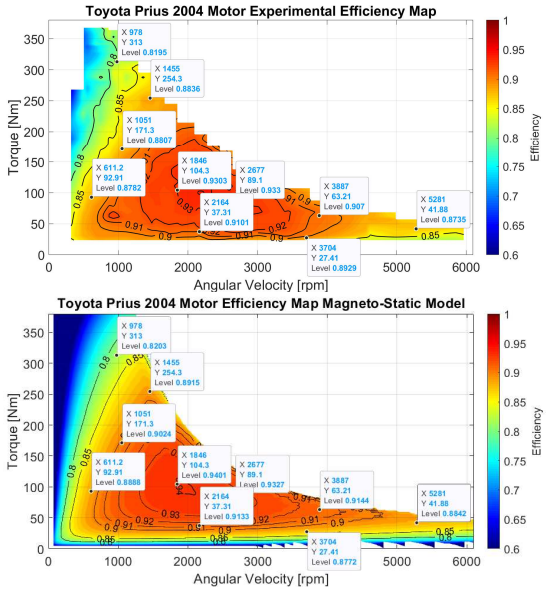

Fig. 7. (a) Toyota Prius 2004 PMSM experimental efficiency map. (b) Toyota Prius 2004 PMSM magneto-static model efficiency map.

TABLE II
EXPERIMENTAL VS MAGNETO-STATIC EFFICIENCY MAP COMPARISON

Regime Characteristics		**Isostatic model Efficiency (p.u)**	**Experimental Efficiency (p.u)**	**Relative error (%)**
Angular velocity (rpm)	Torque (Nm)			
611.2	92.91	0.8888	0.8780	1.23
1051	171.3	0.9024	0.8807	2.46
978	313	0.8203	0.8195	0.10
1455	254.3	0.8915	0.8836	0.89
1846	104.3	0.9401	0.9303	1.05
2164	37.31	0.9133	0.9101	0.35
2677	89.1	0.9327	0.9330	0.03
3704	27.41	0.8772	0.8929	1.75
3887	63.21	0.9144	0.9070	0.82
5281	41.88	0.8842	0.8735	1.22

According to the values presented in Table II, the relative error of the experimental efficiencies and those obtained by means of the proposed method is below 2% in the whole torque-speed plane. As explained, the normalized SSIM index compares the similitude between two images, in this case the experimental efficiency-torque-speed maps and the one obtained by means of the approach proposed in this paper. The SSIM index from the comparison of Figs. 7 (a) and 7 (b) is 0.958. This difference of 0.042 is due to the error contained by the Magneto-Static FEA and the implicit errors due the same experimental results.

As the iron losses are the most complex component of the power losses to calculate, the iron losses obtained from magneto-static FEA are compared with those calculated using time-dependent FEA. These results are summarized in Table III, which shows different randomly chosen operating conditions and the error between both methods.

Finally, in order to validate the iron losses using the Toyota Prius 2004 experimental results, some transformations were done to obtain the magnetic losses using the experimental efficiency map. Three parameters available from the experimental data, i.e., efficiency, stator current and winding temperature, from which copper losses can be obtained. On the other hand, experimental mechanical losses are also available. Considering such data, the experimental iron losses can be calculated as,

$$P_{Fe} = P_U / \eta - P_U - P_{Cu} - P_{ML} \tag{16}$$

TABLE III
MAGNETO-STATIC VS TIME-DEPENDENT FEA MAGNETIC LOSSES COMPARISON

Regime Characteristics			**Magneto Static ML Model (W)**	**Time Dependent ML Model (W)**	**Relative error (%)**
Angular velocity (rpm)	*d*-axis current (A)	*q*-axis current (A)			
431.3	-101.1	106.1	38.61	36.31	6.33
1479	-28.47	45.88	128.74	121.16	6.26
4005	-69.25	23.97	597.43	585.73	2.00
4005	-132.1	27.65	947.82	921.47	2.86
5792	-114.3	18.28	1584.14	1680.78	5.75
6038	-79.28	16.59	1299.93	1348.71	3.62

Fig. 8 (a) shows the resulting iron losses calculated from the experimental data. Fig. 8 (b) shows the iron losses calculated from the magneto-static FEA model.

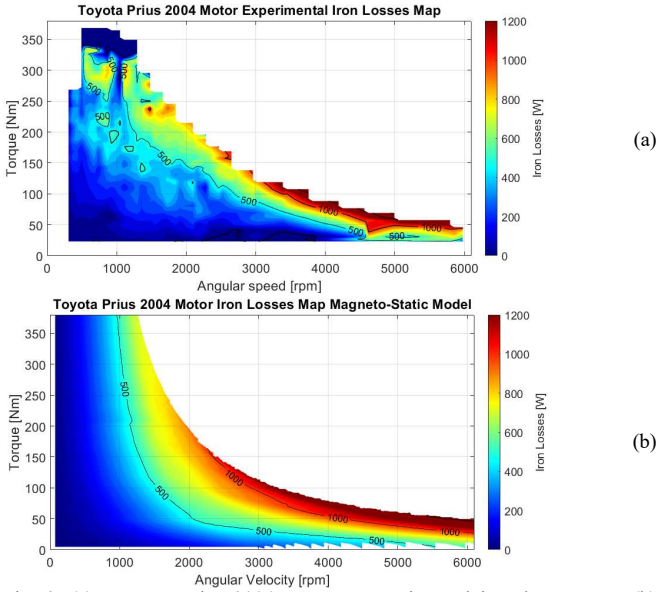

Fig. 8. (a) Toyota Prius 2004 PMSM. Experimental iron losses map. (b) Toyota Prius 2004 PMSM. Magneto-static iron losses map.

As can be observed in Fig. 8, both maps show a great similarity, and thus, the proposed magneto-static FEA model is validated. Therefore, it is concluded that the model is suitable to be used as a design tool to be included within an iterative optimization strategy.

VI. PMSM DESIGN AND OPTIMIZATION VALIDATION

The experimental data of the PMSM of the Toyota Prius 2004 [15] and the Toyota Camry [16] are used to validate the design-optimization process together with the proposed magneto-static FEA and *d-q* electrical model, which were validated in the previous section. First, a seed geometry is defined. Due to space constraints, the outer stator diameter is constant during the optimization process, whereas the shaft diameter is constant due the torque requirements. Other

parameters (h_{brg}, h_{rib}, h_{so}, w_{so}, w_{brg}) are kept constant since the values calculated during the pre-design process guarantee the mechanical robustness and winding process feasibility. These parameters have little impact on the optimization process.

Table IV shows the values of the constant parameters against the reference values of the Toyota Prius 2004 and Camry 2007 PMSMs obtained from public data. The experimental torque-speed-efficiency maps found in [15] and [16] have been used as the target map.

TABLE IV
TOYOTA PRIUS/CAMRY GEOMETRY CONSTANT PARAMETERS COMPARISON

Geometry Parameter	Seed values Prius/Camry	Optimized values Prius/Camry	Reference values Prius/Camry
h_{brg} [mm]	1.5/2.0	1.5/2.0	1.65/2.04
h_{rib} [mm]	2.5/0	2.5/0	2.8/0
h_{so} [mm]	1.0/1.0	1.0/1.0	1.1/1.02
w_{brg} [mm]	2.0/3.5	2.0/3.5	2.09/3.8
w_{so} [mm]	2.0/2.0	2.0/2.0	1.93/1.88
w_{web}[mm]	0/1.5	0/1.5	0/1.65

The optimization parameters range is set by the designer considering space constrains and manufacturing tolerances. Therefore, this strategy allows validating the performance of the design-optimization method by obtaining the PMSMs geometries closest to the original ones.

A. *Validation Analyzing Toyota Prius 2004 PMSM*

Table V summarizes the seed values of the parameters as well as the geometry obtained after the optimization process, in order to compare the obtained values of the geometrical parameters with those of the original Toyota Prius 2004 PMSM.

TABLE V
TOYOTA PRIUS 2004. GEOMETRIC PARAMETERS COMPARISON

Parameter	Seed value	Lower/upper optimization bounds	Optimized geometry	Toyota Prius geometry	Error (%)
g [mm]	1	0.2/1.5	0.747	0.75	0.40
D_{or} [mm]	190	115/230	161.38	160.5	0.55
h_t [mm]	20	5/60	32.84	33.5	1.97
w_t [mm]	4	2/10	7.51	7.6	1.18
h_{sy} [mm]	18.6	5/60	20.32	20.1	1.09
h_{PM} [mm]	8	3/10	6.77	6.5	4.15
w_{PM} [mm]	15	10/25	17.61	18	2.17
L [mm]	60	1/300	81.59	83.6	2.40
N_{ph}	100	8/200	80	72	11.11
d_{wire} [mm^2]	0.85	0.5/1.5	0.89	0.91	2.20
α_{PM} [°]	95.3	90/180	135.75	145	6.38

As observed in Table V, the geometry obtained through the design-optimization process matches with the original one with fidelity. The highest divergence is observed in the number of turns per phase, which is due to a difference of one conductor per slot with respect to the original configuration. It has little effect on the torque-speed-efficiency maps because the optimization compensates this extra conductor per slot by decreasing the magnet size and the stack length of the optimized solution, thus resulting in similar torque and speed capabilities.

Fig. 10 (a) shows the torque-speed-efficiency map of the seed geometry, whereas Fig. 10 (b) shows the map of the optimized solution.

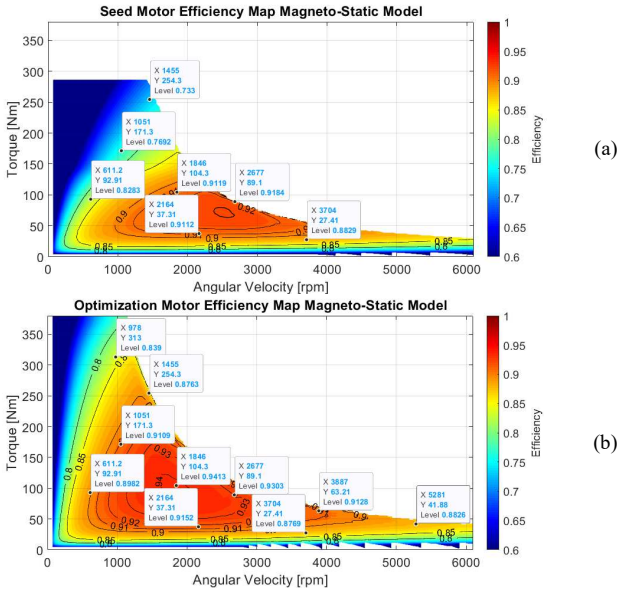

Fig. 10. (a) Torque-speed-efficiency map of the seed geometry. (b) Torque-speed-efficiency map of the optimized geometry.

Table VI compares the efficiency in different operating points of the optimized machine versus the experimental efficiency of the Toyota Prius 2004 PMSM.

TABLE VI
EXPERIMENTAL VS DESIGN-OPTIMIZATION MAGNETO-STATIC EFFICIENCY MAP COMPARISON OF TOYOTA PRIUS 2004

Regime characteristics		Optimized geometry efficiency (p.u)	Experimental efficiency (p.u)	Relative error (%)
Angular velocity (rpm)	Torque (Nm)			
611.2	92.91	0.8982	0.8780	2.30
1051	171.3	0.9109	0.8807	3.43
978	313	0.8390	0.8195	2.38
1455	254.3	0.8763	0.8836	0.83
1846	104.3	0.9413	0.9303	1.18
2164	37.31	0.9152	0.9101	0.56
2677	89.1	0.9303	0.9330	0.29
3704	27.41	0.8769	0.8929	1.79
3887	63.21	0.9128	0.9070	0.64
5281	41.88	0.8826	0.8735	1.04

The relative errors displayed in Table VI allow validating the design-optimization process proposed in this work.

The SSIM index resulting from the comparison of the seed torque-speed-efficiency map and the experimental one is 0.701, whereas the SSIM index between the torque-speed-efficiency map of the optimized motor and the experimental one is 0.929.

B. *Validation Analyzing Toyota Camry 2007 PMSM*

Table VII shows the seed values of the parameters as well as the geometry obtained after the optimization process, in order to compare the obtained values of the geometrical parameters with those of the original Toyota Camry 2007 PMSM. As observed in Table VII, the geometry obtained through the design-optimization process matches with the original one with fidelity.

TABLE VII
TOYOTA CAMRY 2007. GEOMETRIC PARAMETERS COMPARISON

Parameter	Seed value	Lower/upper optimization bounds	Optimized geometry	Toyota Camry geometry	Error (%)
g [mm]	1	0.2/1.5	0.738	0.75	1.60
D_{or} [mm]	190	115/230	162.203	160.5	1.06
h_t [mm]	20	5/60	28.97	30.9	6.25
w_t [mm]	4	2/10	7.613	7.6	0.17
h_{sy} [mm]	18.6	5/60	21.2	20.1	5.47
h_{PM} [mm]	8	3/10	6.477	6.6	1.86
w_{PM} [mm]	15	10/25	18.42	19.1	3.56
L [mm]	40	1/300	62.311	60.6	2.82
N_{ph}	80	8/200	56	56	0.00
d_{wire} [mm^2]	0.63	0.5/1.5	0.881	0.812	8.50
α_{PM} [°]	95	90/180	141.59	145	2.35

Fig. 11 (a) shows the experimental torque-speed-efficiency map, Fig. 11 (b) shows the torque-speed-efficiency map evaluated with the FEA magneto-static model, whereas Fig. 11 (c) shows the optimized motor torque-speed-efficiency map of the Toyota Camry 2007.

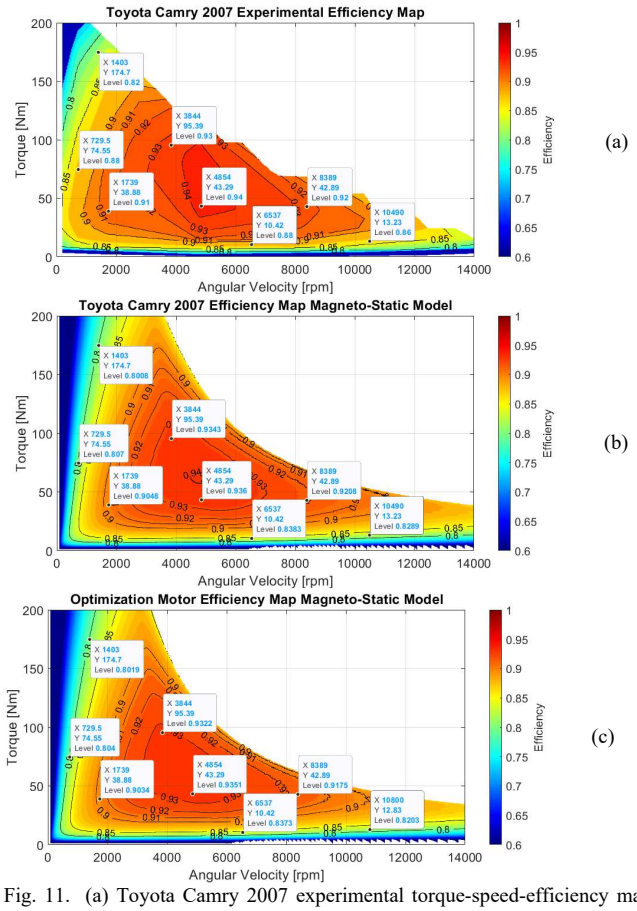

Fig. 11. (a) Toyota Camry 2007 experimental torque-speed-efficiency map. (b) Toyota Camry 2007 magneto-static model torque-speed-efficiency map. (c) Optimized motor torque-speed-efficiency map.

When the original Toyota Camry 2007 PMSM is analyzed by means of the magneto-static model, the SSIM between the torque-speed-efficiency map of the actual geometry when analyzed by the FEA model and the experimental one is 0.9695, thus validating the accuracy of the FEA model. The SSIM index between the seed torque-speed-efficiency map and the experimental one is 0.7978, whereas the SSIM index between the torque-speed-efficiency map of the optimized motor and the experimental one is 0.9571.

C. Target Completion of Toyota Prius and Camry PMSMs

A target completion degree of 5% calculated through the SSIM index is settled as the deviation between the optimized and the original geometries of the Toyota Prius 2004 and Camry 2007 PMSMs.

In the case of the Toyota Prius 2004 PMSM, the actual geometry when analyzed by the FEA model has a SSIM of 0.958, whereas the optimized motor has a SSIM of 0.929, thus resulting a deviation of 3.03%. In the case of the Toyota Camry 2007 PMSM, the deviation is only 1.28%.

Fig. 12 shows the *patternsearch* optimization convergence for both cases, showing the seed value and the optimum convergence.

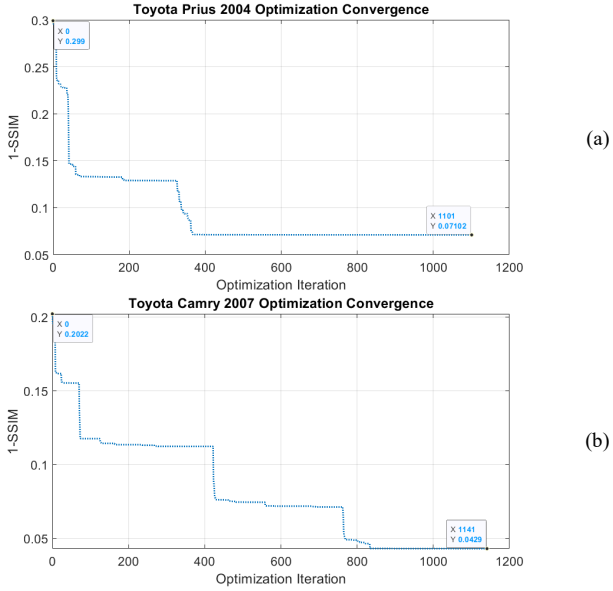

Fig. 12. (a) Toyota Prius 2004 *patternsearch* optimization convergence. (b) Toyota Camry 2007 *patternsearch* optimization convergence.

As observed in Fig. 12, the optimization required around 1100 solver iterations for both PMSMs to find the nearest geometry solution.

D. Computational burden

For the PMSMs analyzed, the design-optimization algorithm shown in Fig. 1 requires 30-40 seconds to perform one iteration, depending on the saturation conditions of the machine. The *pattern search* optimizer available in Matlab® required 5 days in both cases to find the optimum solution, when limiting the number of function evaluations to 10000 using an Intel® Core™ i9-7940X 3.10 GHz processor with 64 GB RAM memory. This time is reasonable, since this strategy allows obtaining an optimized machine, thus avoiding several iterations to manufacture the prototype and saving time, labor and manufacturing costs.

VII. CONCLUSIONS

This paper has presented a novel methodology for designing and optimizing permanent magnet synchronous motors (PMSM) by combining magneto-static FEA and direct-

quadrature (*d-q*) electrical modeling, thus greatly reducing the computational burden when compared to conventional methods based on time-dependent FEA.

The input of the optimization algorithm is the torque-speed-efficiency map of the target motor, so that, the design-optimization process searches the motor geometry that better approximates its torque-speed-efficiency map to the target one. The comparison between maps is computed through an image comparison technique called structural similarity index (SSIM).

The method for calculating the torque-speed-efficiency map is based on magneto-static FEA combined with (*d-q*) electrical modeling. It takes into account iron, mechanical and copper losses. Iron losses consider the harmonic content of the magnetic flux density by applying the time-space conversion.

First, the accuracy of the torque-speed-efficiency maps obtained by means of the proposed magneto-static FEA method combined with a *d-q* electrical model was validated. To this end, the public experimental data of the Toyota Prius 2004 PMSM was used, and the torque-speed-efficiency map of the original PMSM geometry calculated through the proposed methodology was compared with the experimental one. Results presented in this paper show the high accuracy of the magneto-static FEA method combined with the *d-q* electrical model.

Finally, once the magneto-static FEA model was validated, the accuracy of the whole design-optimization algorithm method was assessed by using the experimental torque-speed-efficiency maps of the Toyota Prius 2004 and Toyota Camry 2007 PMSMs as target objectives. It was found that the geometries obtained in both cases through the optimization process were very similar to these of the original machines, thus confirming the accuracy of the proposed design-optimization method.

VIII. Acknowledgments

The authors would like to thank the support of the Generalitat de Catalunya under the Industrial Doctorate 2018 DI 004 and 2017SGR0967 projects, as well as the Spanish Ministry of Economy and Competitiveness under the project TRA2016-80472-R.

IX. References

[1] J. Pyrhonen, T. Jokinen, and V. Hrabovcová, *Design of rotating electrical machines*, 2nd edn. Hoboken: Wiley, 2013.

[2] H. Jung, D. Kim, C. B. Lee, J. Ahn, and S. Y. Jung, "Numerical and experimental design validation for adaptive efficiency distribution compatible to frequent operating range of IPMSM," *IEEE Trans. Magn.*, vol. 50, no. 2, Feb. 2014.

[3] J. Du, X. Wang, and H. Lv, "Optimization of Magnet Shape Based on Efficiency Map of IPMSM for EVs," *IEEE Trans. Appl. Supercond.*, vol. 26, no. 7, Oct. 2016.

[4] C. Lopez-Torres, A. Garcia Espinosa, J.-R. Riba, and L. Romeral, "Design and Optimization for Vehicle Driving Cycle of Rare-Earth-Free SynRM Based on Coupled Lumped Thermal and Magnetic Networks," *IEEE Trans. Veh. Technol.*, vol. 67, no. 1, pp. 196–205, Jan. 2018.

[5] C. Lopez-Torres, A. Garcia, J.-R. Riba, G. Lux, and L. Romeral, "Computationally Efficient Design and Optimization Approach of PMa-SynRM in Frequent Operating Torque–Speed Range," *IEEE Trans. Energy Convers.*, vol. 33, no. 4, pp. 1776–1786, Dec. 2018.

[6] D. M. Ionel and M. Popescu, "Ultrafast finite-element analysis of brushless PM machines based on space-time transformations," *IEEE Trans. Ind. Appl.*, vol. 47, no. 2, pp. 744–753, Mar. 2011.

[7] V. Ruuskanen, J. Nerg, J. Pyrhonen, S. Ruotsalainen, and R. Kennel, "Drive cycle analysis of a permanent-magnet traction motor based on magnetostatic finite-element analysis," *IEEE Trans. Veh. Technol.*, vol. 64, no. 3, pp. 1249–1254, Mar. 2015.

[8] X. Wang, T. D. Strous, D. Lahaye, H. Polinder, and J. A. Ferreira, "Modeling and Optimization of Brushless Doubly-Fed Induction Machines Using Computationally Efficient Finite-Element Analysis," *IEEE Trans. Ind. Appl.*, vol. 52, no. 6, pp. 4525–4534, Nov. 2016.

[9] H. Chen, X. Liu, N. A. O. Demerdash, A. M. El-Refaie, Z. Chen, and J. He, "Computationally efficient optimization of a five-phase flux-switching PM machine under different operating conditions," *IEEE Trans. Veh. Technol.*, vol. 68, no. 7, pp. 6495–6508, Jul. 2019.

[10] L. Xu, W. Zhao, G. Liu, and C. Song, "Design Optimization of a Spoke-Type Permanent-Magnet Vernier Machine for Torque Density and Power Factor Improvement," *IEEE Trans. Veh. Technol.*, vol. 68, no. 4, pp. 3446–3456, Apr. 2019.

[11] H. Fang and D. Wang, "A Novel Design Method of Permanent Magnet Synchronous Generator from Perspective of Permanent Magnet Material Saving," *IEEE Trans. Energy Convers.*, vol. 32, no. 1, pp. 48–54, Mar. 2017.

[12] X. Sun, Z. Shi, G. Lei, Y. Guo, and J. Zhu, "Analysis and Design Optimization of a Permanent Magnet Synchronous Motor for a Campus Patrol Electric Vehicle," *IEEE Trans. Veh. Technol.*, vol. 68, no. 11, pp. 10535–10544, Nov. 2019.

[13] H. C. Jung, G. J. Park, D. J. Kim, and S. Y. Jung, "Optimal Design and Validation of IPMSM for Maximum Efficiency Distribution Compatible to Energy Consumption Areas of HD-EV," *IEEE Trans. Magn.*, vol. 53, no. 6, Jun. 2017.

[14] C. T. Krasopoulos, M. E. Beniakar, and A. G. Kladas, "Multicriteria PM motor design based on ANFIS evaluation of EV driving cycle efficiency," *IEEE Trans. Transp. Electrif.*, vol. 4, no. 2, pp. 525–535, Jun. 2018.

[15] R. H. Staunton, C. W. Ayers, L. D. Marlino, J. N. Chiasson, and B. A. Burress, "Evaluation of 2004 Toyota Prius Hybrid Electric Drive System," Oak Ridge, TN (United States), May 2006.

[16] T. A. Burress *et al.*, "Evaluation of the 2007 Toyota Camry Hybrid Synergy Drive System," Oak Ridge, TN (United States), Apr. 2008.

[17] Z. Wang, A. C. Bovik, H. R. Sheikh, and E. P. Simoncelli, "Image Quality Assessment: From Error Visibility to Structural Similarity," *IEEE Trans. Image Process.*, vol. 13, no. 4, pp. 600–612, Apr. 2004.

[18] F. Verbelen, A. Abdallh, H. Vansompel, K. Stockman, and P. Sergeant, "Sizing Methodology Based on Scaling Laws for a Permanent Magnet Electrical Variable Transmission," *IEEE Trans. Ind. Electron.*, vol. 67, no. 3, pp. 1739–1749, Mar. 2020.

[19] N. Bianchi, T. M. Jahns, and W. . (2004. 10. 05. (Seattle, *Design, analysis, and control of interior PM synchronous machines : tutorial course notes ; Seattle, Oct. 5, 2004*. CLEUP, 2004.

[20] C. Candelo-Zuluaga, A. G. Espinosa, J.-R. Riba, P. T. Blanch, and F. J. Descalzo, "Water-Pumping Permanent Magnet Synchronous Motor Optimization Based on Customized Torque-Speed Operating Area and Performance Characteristics," 2019, pp. 1471–1476.

[21] A. Mahmoudi, W. L. Soong, G. Pellegrino, and E. Armando, "Loss Function Modeling of Efficiency Maps of Electrical Machines," *IEEE Trans. Ind. Appl.*, vol. 53, no. 5, pp. 4221–4231, Sep. 2017.

[22] C. Lopez-Torres, C. Colls, A. Garcia, J.-R. Riba, and L. Romeral, "Development of a Behavior Maps Tool to Evaluate Drive Operational Boundaries and Optimization Assessment of PMa-SynRMs," *IEEE Trans. Veh. Technol.*, vol. 67, no. 8, pp. 6861–6871, Aug. 2018.

[23] S. Stipetic, J. Goss, D. Zarko, and M. Popescu, "Calculation of Efficiency Maps Using a Scalable Saturated Model of Synchronous Permanent Magnet Machines," *IEEE Trans. Ind. Appl.*, vol. 54, no. 5, pp. 4257–4267, Sep. 2018.

X. BIOGRAPHIES

Carlos Candelo-Zuluaga received the M.S. in industrial engineering from the Universitat Politècnica de Catalunya, Barcelona, Spain. Where he is currently working toward the Ph.D. degree in electrical engineering. His research interest includes the design and optimization of permanent magnet synchronous motors.

Antonio Garcia received the M.S. degree in electrical engineering and the Ph.D. degree from the Universitat Politècnica de Catalunya, in 2000 and 2005, respectively. He is with the Motion and Industrial Control Research Group (MCIA). His research interests include electromagnetic devices, electric machines, variable-speed drive systems, and fault-detection algorithms.

Jordi-Roger Riba (M'09) was born in Igualada, Spain, in 1966. He received the M.S. and Ph.D. degrees in physics from the Universitat de Barcelona, Barcelona, Spain, in 1990 and 2000, respectively. In 1992, he joined the Universitat Politècnica de Catalunya, where he is currently a Full professor. He is currently with the Motion Control and Industrial Applications Research Group (MCIA). His current research interests include modeling and simulation of electromagnetic devices, electrical machines and high-voltage engineering.

Pere Tubert Blanch was born in Crespià, Spain, in 1966. He received the mechanical engineering degree from the Universitat Politècnica de Catalunya in 1988. He joined to ESPA corporation at 1989 being the technical and quality director while implementing ISO 9001. He is currently working as a mechanical designer in Midtal Talentos S.L company.